Evaluation of sediment and 137Cs redistribution in the Oginosawa River catchment near the Fukushima Dai-ichi Nuclear Power Plant using integrated watershed modeling

Kazuyuki Sakuma, [*a, d] Alex Malins, [b] Hironori Funaki, [a] Hiroshi Kurikami, [a, b] Tadafumi Niizato, [a] Takahiro Nakanishi, [a] Koji Mori, [c] Kazuhiro Tada, [c] Takamaru Kobayashi, [c] Akihiro Kitamura, [a, b] Masaaki Hosomi [d].

[a] Sector of Fukushima Research and Development, Japan Atomic Energy Agency, 10-2 Fukasaku, Miharu-machi, Fukushima 963-7700, Japan

[b] Center for Computational Science & e-Systems, Japan Atomic Energy Agency, University of Tokyo Kashiwanoha Campus Satellite, 178-4-4 Wakashiba, Kashiwa-shi, Chiba 277-0871, Japan

[c] Geosphere Environmental Technology Corporation, 2-1 Kanda-Awajicho, Chiyoda-ku, Tokyo 101-0063, Japan

[d] Department of Chemical Engineering, Tokyo University of Agriculture and Technology, 2-24-16 Naka, Koganei, Tokyo 184-8588, Japan

[*]Corresponding author. E-mail address: sakuma.kazuyuki@jaea.go.jp (K. Sakuma)

Highlights

- Simulation of ^{137}Cs redistribution in the Oginosawa River catchment between May 2011 and December 2015 using GETFLOWS.
- Majority of ^{137}Cs supplied to watercourses in simulation came from forests and paddy fields next to channels.
- Erosion rate of forested areas away from channels (0-10 g m^{-2} y^{-1}) was at least 25 times lower than rate for paddy fields.
- Parts of the catchment were decontaminated between fall 2012 and March 2014.
- Simulation underestimated sediment discharge up to October 2014, suggesting fast erosion occurred after decontamination.

Abstract

The Oginosawa River catchment lies 15 km south-west of the Fukushima Dai-ichi nuclear plant and covers 7.7 km^2. Parts of the catchment were decontaminated between fall 2012 and March 2014 in preparation for the return of the evacuated population. The General-purpose Terrestrial Fluid-flow Simulator (GETFLOWS) code was used to study sediment and ^{137}Cs redistribution within the catchment, including the effect of decontamination on redistribution. Fine resolution grid cells were used to model local features of the catchment, such as paddy fields adjacent to the Oginosawa River. The simulation was verified using monitoring data for river water discharge rates (r = 0.92), suspended sediment concentrations, and particulate ^{137}Cs concentrations (r = 0.40). Cesium-137 input to watercourses came predominantly from land adjacent to river channels and forest gullies, e.g. the paddy fields in the Ogi and Kainosaka districts, as the ground in these areas saturates during heavy rain and is easily eroded. A discrepancy between the simulation and monitoring results on the sediment discharge rate following decontamination may be explained by fast erosion occurring after decontamination. Forested areas far from the channels only made a minor contribution to ^{137}Cs input to watercourses, total erosion of between 0.001-0.1 mm from May 2011 to December 2015, as ground saturation is infrequent in these areas. The 2.3-6.9% y^{-1} decrease in the amount of ^{137}Cs in forest topsoil over the study period can be explained by radioactive decay (approximately 2.3% y^{-1}), along with a migration downwards into subsoil and a small amount of export. The amount of ^{137}Cs available for release from land adjacent to rivers is expected to be lower in future than compared to this study period, as the simulations indicate a high depletion of inventory from these areas by the end of 2015. However continued monitoring of ^{137}Cs concentrations in river water over future years is advised, as recultivation of paddy fields by returnees may again lead to fast erosion rates and release of the remaining inventory.

1. Introduction

The accidents at the Fukushima Dai-ichi Nuclear Power Plant (FDNPP) in March 2011 contaminated large parts of North-East Japan (Chino et al., 2011; Stohl et al., 2012; Terada et al., 2012). Currently the main radioactive contaminant within the environment is ^{137}Cs, which has a half-life of 30.1 y and binds strongly to clays in soil (Akai et al., 2013; Kozai et al., 2012; Tanaka et al., 2013). In river catchments in Fukushima Prefecture ^{137}Cs redistribution occurs by erosion of soil and transport of sediments in surface runoff, and by dissolution within surface and subsurface water flows. In the early years after the accident a large fraction of the transport occurred in the dissolved form (Nagao et al., 2013; Ueda et al., 2013; Yamashiki et al., 2014; Evrard et al., 2015). The fate of ^{137}Cs transported by suspended sediments is either deposition within the downstream catchment or export to the Pacific Ocean (Tanaka et al., 2015). Much of the redistribution of sediment bound ^{137}Cs occurs over typhoons (Nagao et al., 2013; Chartin et al., 2013; Yamashiki et al., 2014; Yamasaki et al., 2016).

One effect of the deposition of sediment bound ^{137}Cs on river and reservoir beds, and its export to the Pacific Ocean, is to reduce contamination levels on the land surface (Evrard et al., 2014). Tracking this process is expensive however as monitoring must be undertaken frequently in many locations. By comparison simulations are a more cost-effective way to estimate the amount of ^{137}Cs redistribution that is occurring in Fukushima Prefecture.

It is necessary to simulate both erosion by raindrop impact and by surface water runoff to calculate the amount of ^{137}Cs input to watercourses. Surface runoff depends on the recharge of surface water into groundwater, on ground saturation levels, and on Hortonian processes. Simulation codes need to calculate both surface and subsurface flows in order to correctly evaluate surface flows. The Integrated Hydrology Model (InHM) (Carr and Loague, 2012; Vanderkwaak and Loague, 2001), ParFlow (Frei et al., 2009), HydroGeoSphere (Sciuto and Diekkrüger, 2010) and General-purpose Terrestrial Fluid-flow Simulator (GETFLOWS) (Tosaka et al., 1996; Mori et al., 2015) are examples of codes incorporating full surface-subsurface coupling.

Previously GETFLOWS was used to simulate five river basins surrounding the FDNPP site. Kitamura et al. (2016) evaluated sediment redistribution within the Odaka, Ukedo, Maeda, Kuma and Tomioka River basins, and Sakuma et al. (2017) evaluated

^{137}Cs redistribution in the same basins. The Oginosawa River catchment was studied in this work. This catchment is located within the Tomioka basin and contains the Ogi tributary and the Ogi Dam reservoir (Fig. 1). The catchment is almost entirely covered by forest, however upstream of the Ogi Dam reservoir paddy fields flank the Oginosawa River and in the Ogi and Kainosaka districts. The relative simplicity of the land cover in the catchment and the fact that the catchment remained evacuated over the study period minimizes the number of factors that need to be considered to understand the ^{137}Cs redistribution. Monitoring data for water discharge, sediment concentrations, and particulate ^{137}Cs concentrations in the Ogi Dam reservoir were used to validate the GETFLOWS simulation.

Previously Onishi et al. (2014a; 2014b) studied the Ogi Dam reservoir alone using the 1D Time-dependent One-dimensional Degradation and Migration (TODAM) and the 3D Flow, Energy, Salinity, Sediment Contaminant Transport (FLESCOT) codes. These results revealed the sediment and radiocesium redistribution patterns within the reservoir. Although the GETFLOWS results (Kitamura et al., 2016; Sakuma et al., 2017) cover the whole Oginosawa River catchment, relatively coarse resolution grid cells were used (~100×100 m), which were comparable to the size of Ogi Dam reservoir (~150×400 m). Higher resolution modelling is necessary to capture features such as paddy fields alongside channels in the catchment. Therefore 12.5×12.5 m grid cells were used in this work to model the catchment.

The Japanese Government lifted the evacuation order around the Ogi Dam and its upstream Oginosawa River in June 2016. Decontamination work was conducted in the area prior to 2016 in preparation for the return of evacuees. Previous research has associated decontamination with an increase in the rate of ^{137}Cs redistribution (Evrard et al., 2014). This effect was explained by bare soil surfaces left upon completion of decontamination work undergoing faster erosion in the period after decontamination than if they had remained covered with vegetation.

The purpose of this research was to assess the amount of ^{137}Cs redistribution that occurred in the Oginosawa River catchment over the study period. A goal was to understand the relative contributions of land lying adjacent to channels versus forested areas far from channels to ^{137}Cs input to the watercourses. A further goal was to understand the effect that decontamination work had on soil erosion and sediment transport rates within the catchment.

2. Study area

2.1 Description of the study area

The Oginosawa River catchment covers a 7.7 km^2 area and lies 15 km south-west of the FDNPP (Fig. 1). The catchment drains towards the Takigawa Dam reservoir and the town of Tomioka. The total inventory of ^{137}Cs in this catchment was 5.5 TBq at the Second Airborne Monitoring Survey (NRA, 2011), giving to a mean surface density of 0.71 MBq m^{-2}. Forests cover 92% of the catchment area (primarily Japanese cedar for forestry, as shown in Fig. 2). Other land uses include paddy fields (2%) and industrial sites (1%), which have been abandoned since the FDNPP accident. The rest of the catchment is covered by felled areas of forest and surface water (e.g. the Ogi Dam reservoir). Upstream of the Ogi Dam reservoir paddy fields lie adjacent to the Oginosawa River in the districts of Ogi and Kainosaka. The annual rainfall in the region is 1600 mm, based on the mean of ten years of measurements (2003 to 2012) from the Kawauchi weather monitoring station (JMA, 2015).

Parts of the Oginosawa River catchment were decontaminated between fall 2012 and March 2014 (Ministry of the Environment, 2017). Decontamination involved stripping top soil from paddy fields, grassy areas and gardens, and removing the litter layer from the first 20 m of forests adjacent to residential buildings and roads (Ministry of the Environment, 2015). The total decontaminated area covered ~0.3 km^2, which represents ~4% of the total Oginosawa River catchment area.

2.2 Simulation model and parameters

The simulation code GETFLOWS calculates surface and subsurface water flows, soil erosion, sediment and radiocesium transport over river basins (Tosaka et al., 1996; Mori et al., 2015; Kitamura et al., 2016; Sakuma et al., 2017). Mori et al. (2015) and Sakuma et al. (2017) list the main equations solved by GETFLOWS.

A three dimensional model of the catchment was developed using surface topographic data from the Geospatial Information Authority of Japan (2012), and subsurface geology data from the Geological Survey of Japan (2012). Fig. S1 shows the land surface elevation and the geology or deposit type of the grid blocks in the model.

The model comprises multiple grid blocks on which GETFLOWS solves the equations of fluid, sediment and radiocesium transport. The land surface is divided into 62,109 cells, each approximately 12.5×12.5 m. Vertically there is one air layer, one surface layer, and 28 sub-surface layers. The total number of grid-blocks was thus 1,863,270.

The volume of the Ogi Dam reservoir is 7.16×10^5 m^3 (Japanese Dam Association, 2016). The outlet of the dam is 340 m above sea level. It was assumed that the water inflow and outflow rates for the dam reservoir were equal at all times during the simulation. Tables S1-S6 in the Supplementary Information list various parameters used in the simulation, such as Manning's roughness coefficient (Table S1), raindrop-induced erosion parameters (Table S2), intrinsic permeability and effective porosity (Table S3 and S4), sediment particle size distribution (Table S5), soil detachability index and adhesion (Table S6). The sediment particles had representative diameters of 0.001 mm, 0.01 mm, 0.1 mm, 0.3 mm, 1 mm, and 5 mm. Generally ^{137}Cs is absorbed to fine particle fractions, however all particle fractions need to be simulated to calculate ^{137}Cs concentrations in deposited sediments. The parameters used in this study are identical to those used by Kitamura et al. (2016) and Sakuma et al. (2017).

The results of the Second Airborne Monitoring Survey were used to initialize the ^{137}Cs inventory of the catchment (NRA, 2011). The ^{137}Cs in each grid block was dispersed homogenously within the top 2 cm of surface soil, except for cells normally covered by surface water (e.g. rivers, the Ogi Dam reservoir) where the ^{137}Cs inventory was set to zero. The choice of 2 cm thickness for the surface soil layer was made balancing the competing factors of computational costs and resolution of the layer structure (the thicknesses of the 28 sub-surface layers used are listed in Table S7). The dissolved and sorbed components of the ^{137}Cs inventory were assumed to be in equilibrium at the start of each simulation. A ^{137}Cs distribution coefficient of $K_d = 4.0 \text{ x } 10^5$ L/kg was applied for the fractions with representative diameter of 0.3 mm or smaller. No ^{137}Cs was allowed to sorb to fractions with diameter larger than 0.3 mm.

Evapotranspiration was modelled with the Hamon method (Hamon, 1961) during the pre-equilibration simulation. The energy balance equation at the surface layer was solved during the production simulation. Various meteorological data were used as inputs to the simulation. These included precipitation quantities from the Kawauchi weather station (JMA, 2015) and the radar AMeDAS system (JMA, 2011-2015), air temperature, sunshine duration, and average wind velocity data from the Kawauchi weather station (JMA, 2015), and relative humidity data from the Onahama weather station (JMA, 2015). The air temperature lapse rate was 0.0057°C m^{-1}. The resolution of the radar AMeDAS data is 1 km^2 square zones and 1 day time intervals.

The annual average precipitation and evapotranspiration values were calculated using weather data from 2003 to 2012. These values were applied in the pre-equilibration simulation until the flows reached a steady state. The production simulation reported in this study covers the period May 2011 to December 2015, including Typhoon Roke in September 2011 and Tropical Storm Etau in September 2015.

2.3 Field survey data

2.3.1 Water discharge and suspended solid concentrations in river water

Water discharge surveys were performed in September, October, November and December 2014 at the location shown in Fig. 3(a). Water flow velocities were measured with a portable water current meter, and river depths and widths measured with a 2 m long surveying ruler and a 10 m long tape measure. To monitor the concentration of suspended solid in river water, a turbidity meter logged the turbidity at 10 min intervals from 9th April 2014 to 31th December 2015. The turbidity results were converted into suspended solid concentrations for the river water as follows:

$$\text{SS concentration (mg L}^{-1}\text{)} = 0.874(\text{turbidity (NTU)}) \qquad (1)$$

This equation was derived empirically from five measurement results using linear regression (r^2=0.99).

2.3.2 Cesium-137 concentration in settling particle collected by sediment trap in Ogi Dam reservoir

The ^{137}Cs activity concentration of settling particles was investigated using a sediment trap deployed at Ogi Dam reservoir during 2014 and 2015. The sediment trap was installed at 3.7 m depth at the station shown in Fig. 3(a). An automated sample changer was used to switch 500 ml polypropylene sample bottles. The sediment samples were dried at 105°C for 24 h and packed into 100 mL plastic containers (U-8 type container, AS ONE, Osaka, Japan) prior to gamma spectroscopy measurements for ^{137}Cs activity.

The activity was measured by a Ge-semiconductor detector (GMX40P4-76 germanium detector, Seiko EG&G ORTEC, Tokyo, Japan) coupled with a multi-channel analyzer (MCA7600, Seiko EG&G ORTEC, Tokyo, Japan) and spectrum analysis software (Gamma Studio, Seiko EG&G ORTEC, Tokyo, Japan). Spectroscopy was performed on the sediments samples within the U-8 containers. The efficiency of the detector was calibrated with a multiple gamma-ray emitting standard source (10 radionuclides – Eckert & Ziegler Isotope Products, California, USA), served to the detector in a U-8 container. The detection limit was on the order of 10^1 Bq kg^{-1} with a 1800 s counting period. The ^{137}Cs activity upon measurement was decay-corrected to the sample collection date.

3. Results and discussion

3.1 Validation of surface water flow rates, suspended sediment and ^{137}Cs concentrations in river water

The surface and subsurface water flows under average weather conditions were established by the end of the pre-equilibration simulation. Fig. S2 shows the surface water level after equilibration. The source of the Oginosawa River lies in the south-west of the basin, and the river drains into the Ogi Dam reservoir. The reservoir outflow correctly drains north-east out of the catchment area. Fig. S3 shows streamlines of surface and subsurface flows within the catchment. The surface streamlines match the locations of river channels in reality, as checked by overlaying the simulation results upon satellite photographs. The subsurface flows infiltrate in the upper parts of this catchment and tend to discharge via springs below the Ogi Dam Reservoir into the Tomioka River. Fig. S4 shows contour lines indicating the height of the subsurface water table under ambient conditions.

The panels in Fig. S5 show the recharge and discharge fluxes of groundwater through the land surface. The recharge rate is 3-4 mm d^{-1} for ~96% of the catchment area (mainly the forested and felled areas). The recharge rate for paddy fields is 1-3 mm d^{-1}. Net discharge occurs in a limited number of locations, e.g. along river channels and in the Ogi Dam reservoir. Discharge rates are generally above 30 mm/d at these locations.

The simulation results for the water discharge rate upstream of the Ogi Dam (Fig. 3) (0.016-2.4 m^3/s) were in reasonable agreement with the measurement results between

September and December 2014 (0.070-0.45 m^3/s), as shown in Fig. 4(a). The correlation between these quantities is shown in Fig. 4(b) (r = 0.92). A limitation of this comparison however is that there are only 11 measurement data points.

The suspended sediment concentration at the same location as where the water discharge rates were measured varied between 0.16 mg L^{-1} and 2.2 x 10^3 mg L^{-1} (Fig. 5). The agreement between the simulation results and the measurements was better in the period after October 2014 than in the prior months. The simulation tended to underestimate the suspended sediment concentration by approximately one order of magnitude prior to October 2014. This is possibly because decontamination work conducted in the catchment led to higher soil erosion rates. Bare soil surfaces were left on completion of decontamination of paddy fields, gardens, etc. Rapid soil erosion has been observed under such conditions elsewhere by Lepage et al. (2015).

It is worth noting that the time resolution of atmospheric forcing inputs to the simulation was 1 day. This means there is a tendency to underestimate the instantaneous measurements during storms (Fig. 5). The main storms during this period were Typhoons Phanfone, Vongfong and Nangka and Tropical Storm Etau.

Figure 6 shows simulated ^{137}Cs concentrations in sediments carried through the inlet of Ogi dam reservoir (0.0058-22 kBq/kg), and measured ^{137}Cs concentrations in particles settling within the reservoir (2.2-28 kBq/kg, full data in Table S8). The simulation results are in reasonable agreement with the observation results (r = 0.40, Fig. 6(b)).

3.2 Characteristics of sediment erosion and deposition, and ^{137}Cs redistribution within the simulation

The simulation results for the net change in the soil inventory per year, and the net change over the full study period (May 2011 to December 2015) are shown in Fig. 7 and Fig. S6, respectively. A large amount of sediment erosion occurs in the vicinity of river channels and forest gullies. By comparison, there is almost no net erosion in the forests away from the channels (average erosion rate between 0-10 g m^{-2} y^{-1}, total erosion of between 0.001-0.1 mm from May 2011 to December 2015). This is because the erosion rate is either very low or eroded sediments quickly redeposit again within the forests.

The most significant deposition locations are the Ogi Dam reservoir and river beds. Deposition along rivers occurs in particular at locations where the flow rate drops, such as where river channels widen.

Figure 8 shows the ^{137}Cs inventory remaining in the top 2 cm of soil at the end of the simulation period, December 31, 2015, relative to the initial inventory at the start of the period (May 26, 2011). Radioactive decay accounts for 10% of the reduction in the ^{137}Cs inventory (approximately 2.3% y^{-1}) over the simulation period. Another factor is downward migration (weathering) of ^{137}Cs from the 2 cm topsoil layer into the subsoil. On average, 1.4% y^{-1} of the ^{137}Cs inventory migrated downwards from the top 2 cm layer into the subsoil across the study area.

Most of the forested areas away from the channels show a reduction of ^{137}Cs inventory within the range 10-30% (approximately 2.3-6.9% y^{-1}). As stated, radioactive decay counts for 2.3% y^{-1} of the reduction, while downward migration into subsoil was on average 1.1% y^{-1} for the forest soils. Much larger reductions in the ^{137}Cs inventory were calculated for topsoils adjacent to river channels and forest gullies (10-100%, Fig. 8).

We calculated the total ^{137}Cs discharge from forested areas and from land near to channels separately. In total 4.1 GBq of ^{137}Cs was discharged from forests away from channels over the course of the simulation. This result is one order of magnitude lower than the corresponding result, 53 GBq, for land adjacent to channels (figures decay corrected to May 2011). In conclusion, ^{137}Cs supplied to rivers mainly came from a limited set of locations surrounding the channels. The main land use around channels is forest, followed by paddy fields. The rate of soil erosion from around channels from May 2011 to December 2015 varied from 0.1 cm to over 1 cm as shown in Fig. S6.

The simulations suggest that over 70% of the ^{137}Cs inventory that existed on May 26, 2011 remained within the top 2 cm of soil across the catchment by December 2015. Soil samples taken from forest test sites in Fukushima Prefecture in 2016 confirm that the majority of ^{137}Cs in forest soils remains within the top 5 cm layer (Ministry of Agriculture, Forestry and Fisheries, 2017). The remaining ^{137}Cs inventory in the Oginosawa River catchment presents a potential source of supply to watercourses in future years. However the rate of supply in future will likely be lower than the rate calculated for the 2011 to 2015 period. This is because the availability of readily mobilizable ^{137}Cs will be lower after December 2015 than was previously the case. This is a consequence of the depletion of ^{137}Cs from the top 2 cm of soil adjacent to channels by discharge into rivers, radioactive decay, and downwards migration into subsoil over the study period.

The reasons for high soil erosion and ^{137}Cs discharge adjacent to river channels and forest gullies are as follows. Figure 9 shows groundwater saturation levels over 2011 Typhoon Roke. The land around river channels and forest gullies saturates over parts of the typhoon period (red areas around channels, Fig. 9). This leads to high surface water runoff rates and associated flow induced erosion. The topsoil tends to remain unsaturated in the forested areas far from the channels due to infiltration.

Land steepness on its own is not a sufficient factor to drive soil erosion. Although Hortonian processes occur, it is critical to have high groundwater saturation levels to cause surface runoff and erosion. This can be seen by comparing the net erosion/deposition results in Fig. 7 with Fig. S1(a) showing the topology of the catchment.

The average erosion rates from paddy fields and forests over the study period simulation are 265 g m^{-2} y^{-1} and 10.6 g m^{-2} y^{-1}, respectively. Note the latter figure represents an upper bound for forests far from channels, as the figure includes the results for forests in the vicinity of channels. The erosion rate of paddy fields is therefore at least 25 times higher for forested areas far from channels. Wakahara et al. (2014) reported an erosion rate from normally cultivated paddy fields of 151 g m^{-2} y^{-1}, compared with 658 g m^{-2} y^{-1} for decontaminated paddy fields stripped of 5-10 cm of topsoil. Niizato et al. (2016) reported an erosion rate from a mountainous forest plot far from channels of 12 g m^{-2} y^{-1}. Therefore our simulation results are in reasonable agreement with these observation results.

For the land adjacent to channels, it is difficult to determine the relative contribution of the different land uses (forests and paddy fields) to the total sediment and ^{137}Cs input to rivers. However Laceby et al. (2016) reported that forest sources contributed 17% of particulate matter and cultivated sources (mainly paddy fields) contributed 38% of particulate matter over coastal catchments in Fukushima Prefecture. The remaining source (contribution of 45%) was classified as subsoil, representing channel bank erosion, landslides and erosion from freshly decontaminated soil surfaces.

Although the land use in this study area is mostly forest, there are two large paddy fields near the inlet of the Ogi Dam reservoir (Fig. 2). Chartin et al. (2013), Wakahara et al. (2014), Yoshikawa et al. (2014) and Yoshimura et al. (2016) reported that paddy fields are important for the supply of radiocesium to rivers. Figure 7 shows high erosion of soils from paddy fields near the inlet of the dam. Lepage et al. (2015) noted that the dense grass cover taking hold in abandoned fields will protect against soil erosion in coming years. However the permeability of paddy fields is low, meaning some surface runoff is inevitable during typhoon floods. Moreover, returnees to previously evacuated areas may recultivate paddy fields, increasing the potential for erosion. Further research is needed to determine how much protection wild vegetation growing on abandoned paddy fields provides against erosion.

4. Conclusion

A three-dimensional hydrogeological structure model was developed to simulate water, sediment and ^{137}Cs transport in the Oginosawa River catchment, including over the period it was decontaminated. The catchment received high ^{137}Cs atmospheric deposition in 2011, as it was within the direction of travel of one of the main radioactive plumes from the accident. The modeling employed a sufficiently fine resolution mesh to evaluate localized hydrological results and allow comparison with field monitoring data.

Water fluxes and suspended sediment concentrations calculated for the Oginosawa River were consistent with monitoring results. However the simulation results for suspended sediment concentrations within the Oginosawa River before October 2014 were an order of magnitude lower than measurements. This discrepancy is likely due to decontamination work on paddy fields and residential areas leading to higher sediment run-off rates in 2014 than usual. Simulated particulate ^{137}Cs concentrations in the Ogi Dam reservoir were also consistent with monitoring results.

The simulation results indicate that the main input of ^{137}Cs to rivers comes from land adjacent to the channels. By comparison, there is a lower contribution from forests far from the channels to the contaminant supply. The ground does not saturate readily in these locations during heavy rainfall period, leading to low soil erosion rates. The simulation suggests a 25 times higher rate of erosion of soil from paddy fields than from forests.

The simulation indicates a large amount of discharge of the ^{137}Cs inventory from the top 2 cm of soil on land adjacent to channels over the study period. This result, coupled with the radioactive decay and migration of ^{137}Cs downwards into subsoil that also occurred, suggests that ^{137}Cs discharge will be lower in future years compared to this study period. However the potential recultivation of the paddy fields in future may lead to faster release rates of sediment and ^{137}Cs than is currently the case for these abandoned sites. The difficulty of modelling sediment and ^{137}Cs discharge from paddy fields and land adjacent to channels underlies the importance of field monitoring for quantifying sediment and ^{137}Cs redistribution.

Acknowledgements

We acknowledge members of the Fukushima Environmental Safety Center and the Center for Computational Science & e-Systems for their assistance during this research. We thank K. Yoshimura for reviewing our manuscript and the Geospatial Information Authority of Japan for providing land topography data created from the aerial laser survey.

References

Akai, J., Nomura, N., Matsushita, S., Kudo, H., Fukuhara, H., Matsuoka, S., Matsumoto, J., 2013. Mineralogical and geomicrobial examination of soil contamination by radioactive Cs due to 2011 Fukushima Daiichi Nuclear Power Plant accident. Phys. Chem. Earth 58-60, 57-67. http://dx.doi.org/10.1016/j.pce.2013.04.010

Carr, A., Loague, K., 2012. Physics-Based Simulations of the Impacts Forest Management Practices Have on Hydrologic Response. In *Proceedings of coast redwood forests in a changing California: A symposium for scientists and managers*, 41-51. http://www.fs.fed.us/psw/publications/documents/psw_gtr238/psw_gtr238_041.pdf

Chartin, C., Evrard, O., Onda, Y., Patin, J., Lefevre, I., Ottle, C., Ayrault, S., Lepage, H., Bonte, P., 2013. Tracking the early dispersion of contaminated sediment along rivers draining the Fukushima radioactive pollution plume. Anthropocene 1, 23-34. http://dx.doi.org/10.1016/j.ancene.2013.07.001

Chino, M., Nakayama, H., Nagai, H., Terada, H., Katata, G., Yamazawa, H., 2011. Preliminary estimation of release amounts of 131I and 137Cs accidentally discharged from the Fukushima Daiichi nuclear power plant into the atmosphere. J. Nucl. Sci. Technol. 48, 1129-1134. http://dx.doi.org/10.1080/18811248.2011.9711799

Evrard, O., Chartin, C., Onda, Y., Lepage, H., Cerdan, O., Lefevre, I., Ayrault, S., 2014. Renewed soil erosion and remobilisation of radioactive sediment in Fukushima coastal rivers after the 2013 typhoons. Sci. Rep. 4, 4574. http://dx.doi.org/10.1038/srep04574

Evrard, O., Laceby, J.P., Lepage, H., Onda, Y., Cerdan, O., Ayrault, S., 2015. Radiocesium transfer from hillslopes to the Pacific Ocean after the Fukushima Nuclear Power Plant accident: A review. J. Environ. Radioact. 148, 92-110. http://dx.doi.org/10.1016/j.jenvrad.2015.06.018

Frei, S., Fleckenstein, J.H., Kollet, S.J., Maxwell, R.M., 2009. Patterns and dynamics of river-aquifer exchange with variably-saturated flow using a fully-coupled model. J. Hydrol. 375, 383-393. http://dx.doi.org/10.1016/j.jhydrol.2009.06.038

Geological Survey of Japan, 2012. Geological Survey of Japan, AIST (ed.). 2012. Seamless digital geological map of Japan 1: 200,000. Jul 3, 2012 version. Research Information Database DB084, Geological Survey of Japan, National Institute of Advanced Industrial Science and Technology.

Geospatial Information Authority of Japan, 2012. http://www.gsi.go.jp/ENGLISH/ (accessed 02.24.16).

Hamon, W.R., 1961. Estimating potential evapotranspiration, Proceedings American Society of Civil Engineers. 87(HY 3), 107-120.

Japanese Dam Association, 2016. http://damnet.or.jp/cgi-bin/binranA/All.cgi?db4=0466 (accessed 04.20.16).

Japan Meteorological Agency (JMA), 2015. http://www.jma.go.jp/jma/indexe.html (accessed 02.24.16).

Kitamura, A., Kurikami, H., Sakuma, K., Malins, A., Okumura, M., Machida, M., Mori, K., Tada, K., Tawara, Y., Kobayashi, T., Yoshida, T., Tosaka, H., 2016. Redistribution and export of contaminated sediment within eastern Fukushima Prefecture due to typhoon flooding. Earth Surf. Process. Landforms 41, 1708-1726. http://dx.doi.org/10.1002/esp.3944

Kozai, N., Ohnuki, T., Arisaka, M., Watanabe, M., Sakamoto, F., Yamasaki, S., Jiang, M., 2012. Chemical states of fallout radioactive Cs in the soils deposited at Fukushima Daiichi Nuclear Power Plant accident. J. Nucl. Sci. Technol. 49, 473-478. http://dx.doi.org/10.1080/00223131.2012.677131

Lepage, H., Evrard, O., Onda, Y., Lefevre, I., Laceby, J.P., Ayrault, S., 2015. Depth distribution of cesium-137 in paddy fields across the Fukushima pollution plume in 2013. J. Environ. Radioact. 147, 157-164. http://dx.doi.org/10.1016/j.jenvrad.2015.05.003

Laceby, J.P., Huon, S., Onda, Y., Vaury, V., Evrard, O., 2016. Do forests represent a long-term source of contaminated particulate matter in the Fukushima Prefecture? J. Environ. Manage. http://dx.doi.org/10.1016/j.jenvman.2016.09.020

Ministry of Agriculture, Forestry and Fisheries (MAFF), 2017. http://www.rinya.maff.go.jp/j/kaihatu/jyosen/attach/pdf/H28_jittaihaaku_kekka-1.pdf (accessed 06.15.17).

Ministry of the Environment (MOE), 2015. http://josen.env.go.jp/en/policy_document/pdf/decontamination_report1503_02.pdf (accessed 07.26.17).

Ministry of the Environment (MOE), 2017. http://josen.env.go.jp/area/details/kawauchi.html (accessed 08.01.17).

Mori, K., Tada, K., Tawara, Y., Ohno, K., Asami, M., Kosaka, K., Tosaka, H., 2015. Integrated watershed modeling for simulation of spatiotemporal redistribution of post-fallout radionuclides: Application in radiocesium fate and transport processes derived from the Fukushima accidents. Environ. Model. Softw. 72, 126-146. http://dx.doi.org/10.1016/j.envsoft.2015.06.012

Nagao, S., Kanamori, M., Ochiai, S., Tomihara, S., Fukushi, K., Yamamoto, M., 2013. Export of 134Cs and137Cs in the Fukushima river systems at heavy rains by Typhoon Roke in September 2011. Biogeosciences 10, 6215-6223. http://dx.doi.org/10.5194/bg-10-6215-2013

Niizato, T., Abe, H., Mitachi, K., Sasaki, Y., Ishii, Y., Watanabe, T., 2015. Input and output budgets of radiocesium concerning the forest floor in the mountain forest of Fukushima released from the TEPCO's Fukushima Dai-ichi nuclear power plant accident. J. Environ. Radioact. 161, 11-21. http://dx.doi.org/10.1016/j.jenvrad.2016.04.017

Nuclear Regulation Authority (NRA), 2011. Results of the 2nd Airborne Monitoring by the Ministry of Education, Culture, Sports, Science and Technology and the U.S. Department of Energy. http://radioactivity.nsr.go.jp/en/contents/4000/3165/24/1304797_0616e.pdf (accessed 06.15.17).

Onishi Y., Kurikami H., Yokuda ST., 2014a. Simulation of Sediment and Cesium Transport in the Ukedo River and the Ogi Dam Reservoir during a Rainfall Event using the TODAM Code. http://www.pnnl.gov/main/publications/external/technical_reports/PNNL-23255.pdf (accessed 04.08.16).

Onishi Y., Kurikami H., Yokuda ST., 2014b. Preliminary Three-Dimensional Simulation of Sediment and Cesium Transport in the Ogi Dam Reservoir using FLESCOT - Task 6, Subtask 2. http://www.pnnl.gov/main/publications/external/technical_reports/PNNL-23257.pdf (accessed 16.04.08).

Sakuma K., Kitamura A., Malins A., Kurikami H., Machida M., Mori K., Tada K., Kobayashi T., Tawara Y., Tosaka H., 2017. Characteristics of radio-cesium transport and discharge between different basins near to the Fukushima Dai-ichi Nuclear Power Plant after heavy rainfall events. J. Environ. Radioact. 169-170, 130-150. http://dx.doi.org/10.1016/j.jenvrad.2016.12.006

Sciuto, G., Diekkruger, B., 2010. Influence of Soil Heterogeneity and Spatial Discretization on Catchment Water Balance Modeling. Vadose Zo. J. 9, 955. http://dx.doi.org/10.2136/vzj2009.0166

Stohl, A., Seibert, P., Wotawa, G., Arnold, D., Burkhart, J.F., Eckhardt, S., Tapia, C., Vargas, A., Yasunari, T.J., 2012. Xenon-133 and caesium-137 releases into the atmosphere from the Fukushima Dai-ichi nuclear power plant: Determination of the source term, atmospheric dispersion, and deposition. Atmos. Chem. Phys. 12, 2313-2343. http://dx.doi.org/10.5194/acp-12-2313-2012

Tanaka, K., Sakaguchi, A., Kanai, Y., Tsuruta, H., Shinohara, A., Takahashi, Y., 2013. Heterogeneous distribution of radiocesium in aerosols, soil and particulate matters emitted by the Fukushima Daiichi Nuclear Power Plant accident: Retention of micro-scale heterogeneity during the migration of radiocesium from the air into ground and rive. J. Radioanal. Nucl. Chem. 295, 1927-1937. http://dx.doi.org/10.1007/s10967-012-2160-9

Tanaka, K., Iwatani, H., Sakaguchi, A., Fan, Q., Takahashi, Y., 2015. Size-dependent distribution of radiocesium in riverbed sediments and its relevance to the migration of radiocesium in river systems after the Fukushima Daiichi Nuclear Power Plant accident. J. Environ. Radioact. 139, 390-397. http://dx.doi.org/10.1016/j.jenvrad.2014.05.002

Terada, H., Katata, G., Chino, M., Nagai, H., 2012. Atmospheric discharge and dispersion of radionuclides during the Fukushima Dai-ichi Nuclear Power Plant accident. Part II: Verification of the source term and analysis of regional-scale atmospheric dispersion. J. Environ. Radioact. 112, 141-154. http://dx.doi.org/10.1016/j.jenvrad.2012.05.023

Tosaka, H., Kojima, K., Miki, A., Chino, T., 1996. Numerical Simulation of Surface-Subsurface-Coupled, 2-Phase, 3-Dimensional Fluid Behavior. J. Groundw. Hydrol. 38, 253-267. http://dx.doi.org/10.5917/jagh1987.38.253

Ueda, S., Hasegawa, H., Kakiuchi, H., Akata, N., Ohtsuka, Y., Hisamatsu, S., 2013. Fluvial discharges of radiocaesium from watersheds contaminated by the Fukushima Dai-ichi Nuclear Power Plant accident, Japan. J. Environ. Radioact. 118, 96–104. http://dx.doi.org/10.1016/j.jenvrad.2012.11.009

Vanderkwaak, J.E., Loague, K., 2001. Hydrologic-response simulations for the R-5 catchment with a comprehensive physics-based mode. Water Resour. Res. 37, 999-1013. http://dx.doi.org/10.1029/2000WR900272

Wakahara, T., Onda, Y., Kato, H., Sakaguchi, A., Yoshimura, K., 2014. Radiocesium discharge from paddy fields with different initial scrapings for decontamination after the Fukushima Dai-ichi Nuclear Power Plant accident. Environ. Sci. Process. Impacts 16, 2580-2591. http://dx.doi.org/10.1039/c4em00262h

Yamasaki, S., Imoto, J., Furuki, G., Ochiai, A., Ohnuki, T., Sueki, K., Nanba, K., Ewing, R.C., Utsunomiya, S., 2016. Radioactive Cs in the estuary sediments near Fukushima Daiichi Nuclear Power Plant. Sci. Total Environ. 551-552, 155-162. http://dx.doi.org/10.1016/j.scitotenv.2016.01.155

Yamashiki, Y., Onda, Y., Smith, H.G., Blake, W.H., Wakahara, T., Igarashi, Y., Matsuura, Y., Yoshimura, K., 2014. Initial flux of sediment-associated radiocesium to the ocean from the largest river impacted by Fukushima Daiichi Nuclear Power Plant. Sci. Rep. 4, 3714. http://dx.doi.org/10.1038/srep03714

Yoshikawa, N., Obara, H., Ogasa, M., Miyazu, S., Harada, N., Nonaka, M., 2014. ^{137}Cs in irrigation water and its effect on paddy fields in Japan after the Fukushima nuclear accident. Sci. Total Environ. 481, 252-259. http://dx.doi.org/10.1016/j.scitotenv.2014.01.129

Yoshimura, K., Onda, Y., Wakahara, T., 2016. Time Dependence of the ^{137}Cs

Concentration in Particles Discharged from Rice Paddies to Freshwater Bodies after the Fukushima Daiichi NPP Accident. Environ. Sci. Technol. 50, 4186-4193. http://dx.doi.org/10.1021/acs.est.5b05513

Figure captions

Fig. 1 Cesium-137 contamination density around the FDNPP, including the Tomioka River and the Oginosawa River catchment.

Fig. 2 Land use and land cover of the Oginosawa River catchment.

Fig. 3 Watershed boundary of the study area and monitoring points for water discharge, turbidity in river water and ^{137}Cs concentration in settling particle.

Fig. 4 Simulated and observed water discharge rates for the Oginosawa River. Dotted line in panel (b) is line of equality.

Fig. 5 Simulated and observed suspended sediment concentrations in the Oginosawa River. Peaks occurring during main typhoons in the observation period are highlighted.

Fig. 6 Simulated and observed ^{137}Cs concentrations in suspended sediments in the Ogi Dam reservoir. Dotted line in panel (b) is line of equality.

Fig. 7 Spatial distribution of the net inventory change of soil in the unit of soil mass per area per year (average of results over May 2011 and December 2015).

Fig. 8 Spatial distribution of the remaining ^{137}Cs in the top 2 cm of soil on December 31, 2015, relative to the initial inventory on May 26, 2011 (simulation start date). The inventory of cells normally covered by surface water was set at 0 Bq m^{-2} at the start of the simulation (zero initial inventory), hence no applicable value for residual ^{137}Cs for these cells.

Fig. 9 Distribution of water saturation in the surface soil layer of the model, before, during, and after 2011 Typhoon Roke.

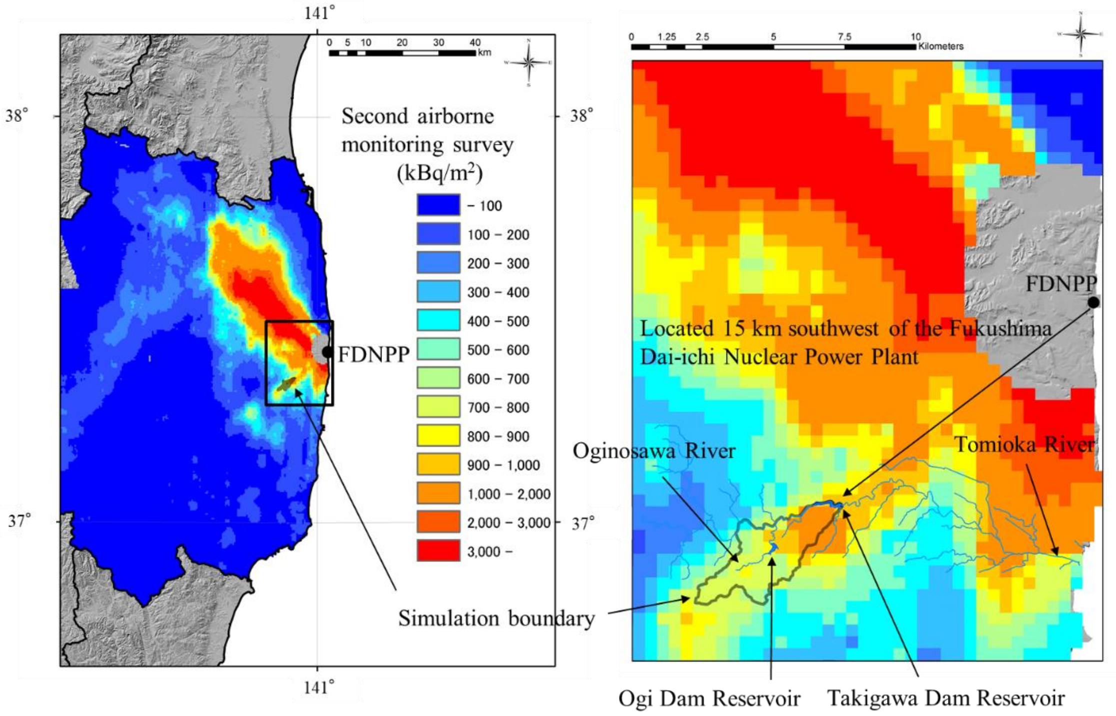

141°
0 5 10 20 30 40 km
38°
38°
Second airborne monitoring survey (kBq/m2)
− 100
100 − 200
200 − 300
300 − 400
400 − 500
500 − 600
600 − 700
700 − 800
800 − 900
900 − 1,000
1,000 − 2,000
2,000 − 3,000
3,000 −
FDNPP
37°
37°
141°
0 1.25 2.5 5 7.5 10 Kilometers
FDNPP
Located 15 km southwest of the Fukushima Dai-ichi Nuclear Power Plant
Oginosawa River
Tomioka River
Simulation boundary
Ogi Dam Reservoir
Takigawa Dam Reservoir

561

562 Fig. 1

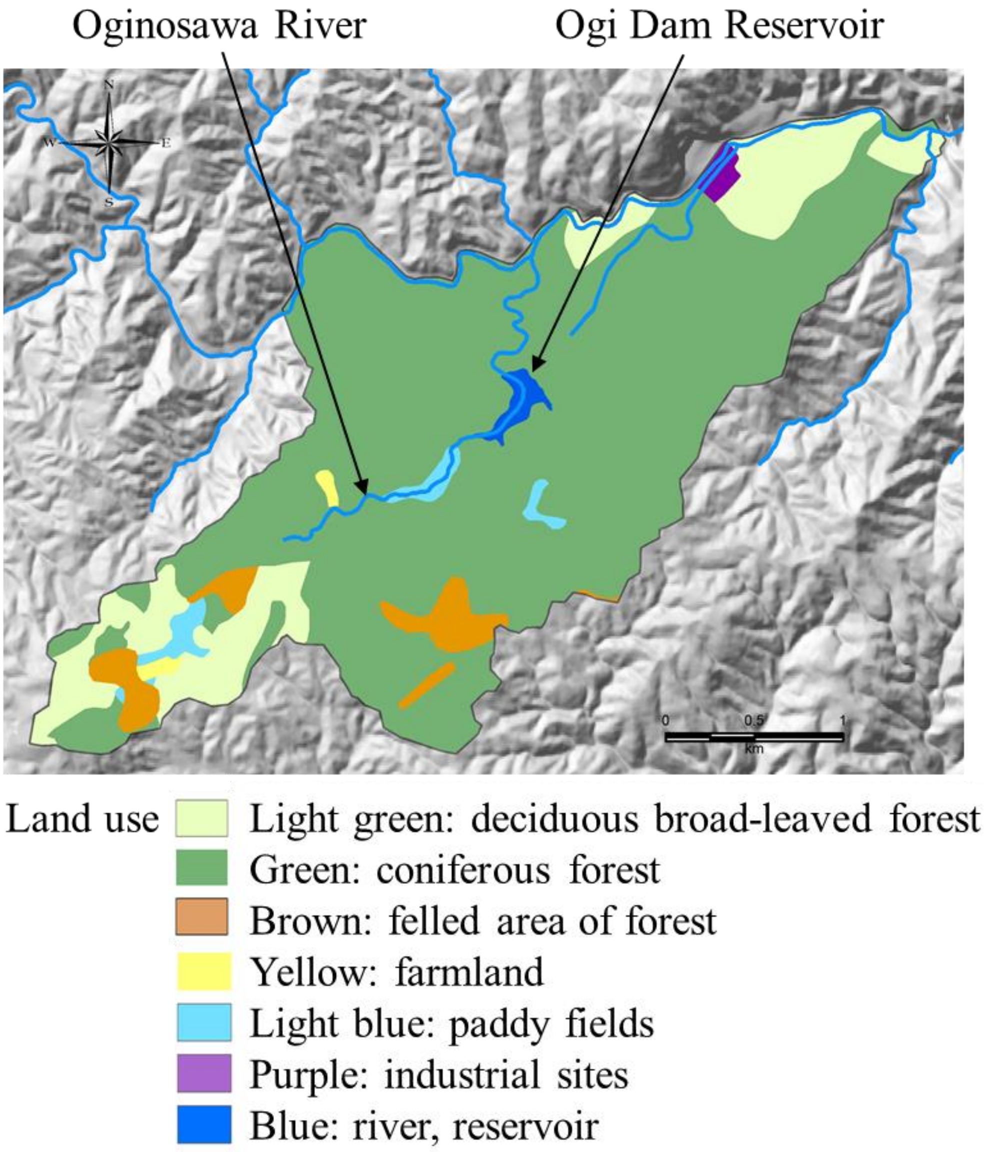
Oginosawa River
Ogi Dam Reservoir
N
W
E
S
0
0.5
1
km
Land use
Light green: deciduous broad-leaved forest
Green: coniferous forest
Brown: felled area of forest
Yellow: farmland
Light blue: paddy fields
Purple: industrial sites
Blue: river, reservoir

Fig. 2

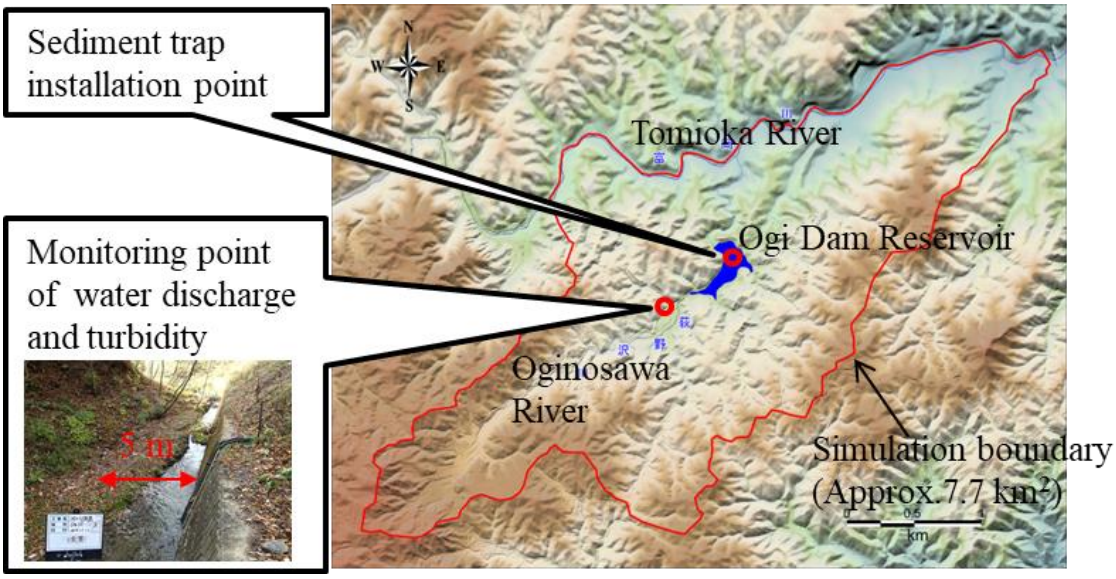
Sediment trap installation point
Monitoring point of water discharge and turbidity
5 m
N
W
E
S
Tomioka River
Ogi Dam Reservoir
Oginosawa River
Simulation boundary (Approx.7.7 km^2)
0
0.5
1
km

Fig. 3

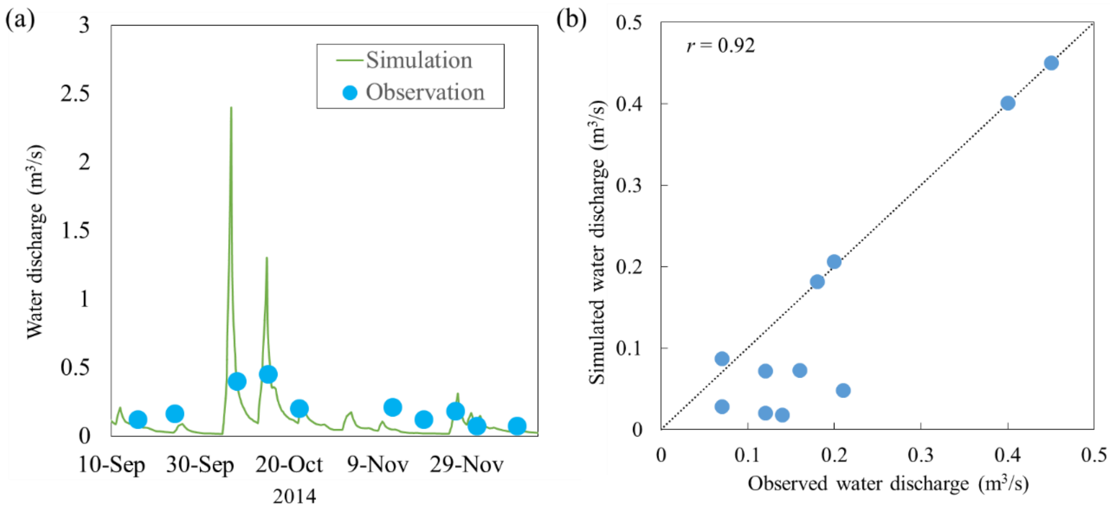
(a)
Water discharge (m^3/s)
3
2.5
2
1.5
1
0.5
0
Simulation
Observation
10-Sep
30-Sep
20-Oct
9-Nov
29-Nov
2014
(b)
Simulated water discharge (m^3/s)
r = 0.92
0.5
0.4
0.3
0.2
0.1
0
Observed water discharge (m^3/s)

Fig. 4

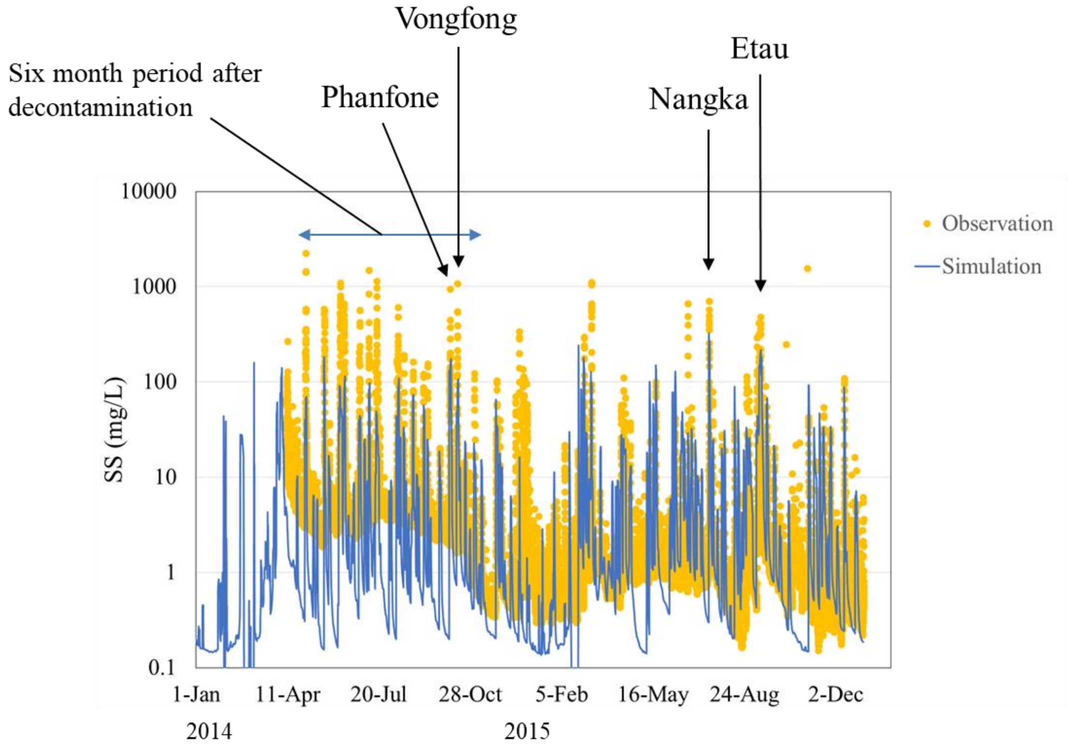
Vongfong
Etau
Six month period after decontamination
Phanfone
Nangka
Observation
Simulation
SS (mg/L)
10000
1000
100
10
1
0.1
1-Jan
11-Apr
20-Jul
28-Oct
5-Feb
16-May
24-Aug
2-Dec
2014
2015

Fig. 5

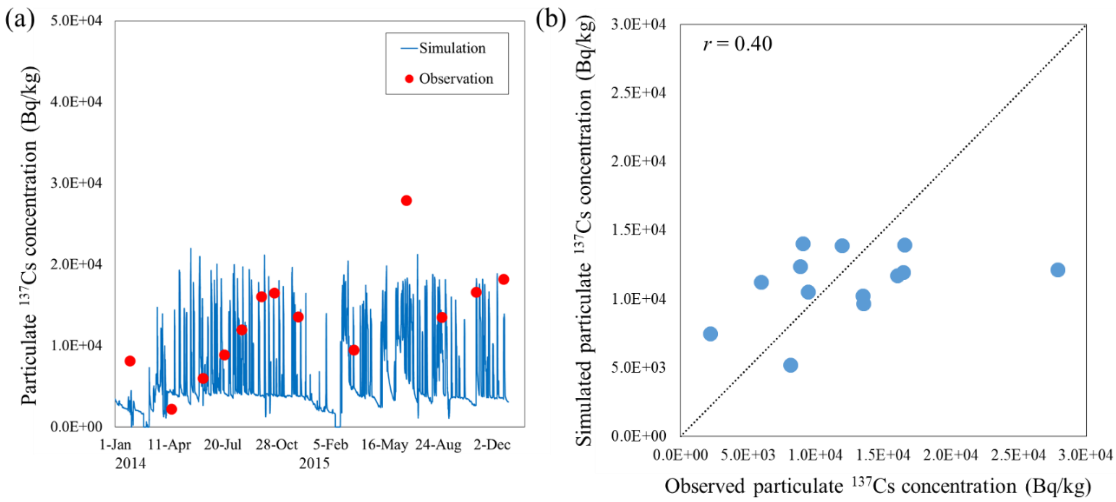
(a)
(b)
Simulation
Observation
Particulate ¹³⁷Cs concentration (Bq/kg)
5.0E+04
4.0E+04
3.0E+04
2.0E+04
1.0E+04
0.0E+00
1-Jan
11-Apr
20-Jul
28-Oct
5-Feb
16-May
24-Aug
2-Dec
2014
2015
r = 0.40
Simulated particulate ¹³⁷Cs concentration (Bq/kg)
3.0E+04
2.5E+04
2.0E+04
1.5E+04
1.0E+04
5.0E+03
0.0E+00
0.0E+00
5.0E+03
1.0E+04
1.5E+04
2.0E+04
2.5E+04
3.0E+04
Observed particulate ¹³⁷Cs concentration (Bq/kg)

Fig. 6

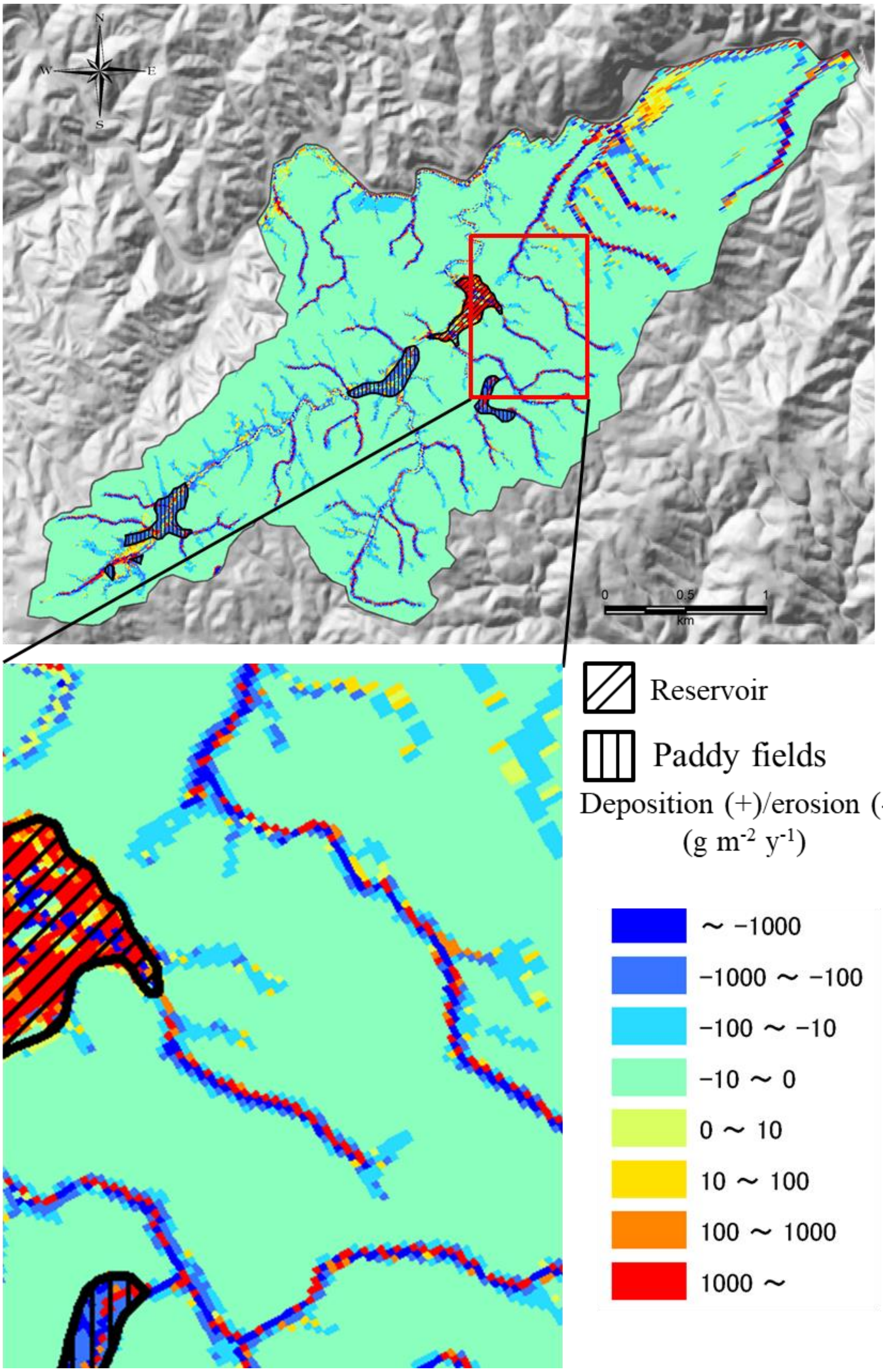
N
W
E
S
0
0.5
1
km
Reservoir
Paddy fields
Deposition (+)/erosion (-)
(g m-2 y-1)
～ −1000
−1000 ～ −100
−100 ～ −10
−10 ～ 0
0 ～ 10
10 ～ 100
100 ～ 1000
1000 ～

Fig. 7

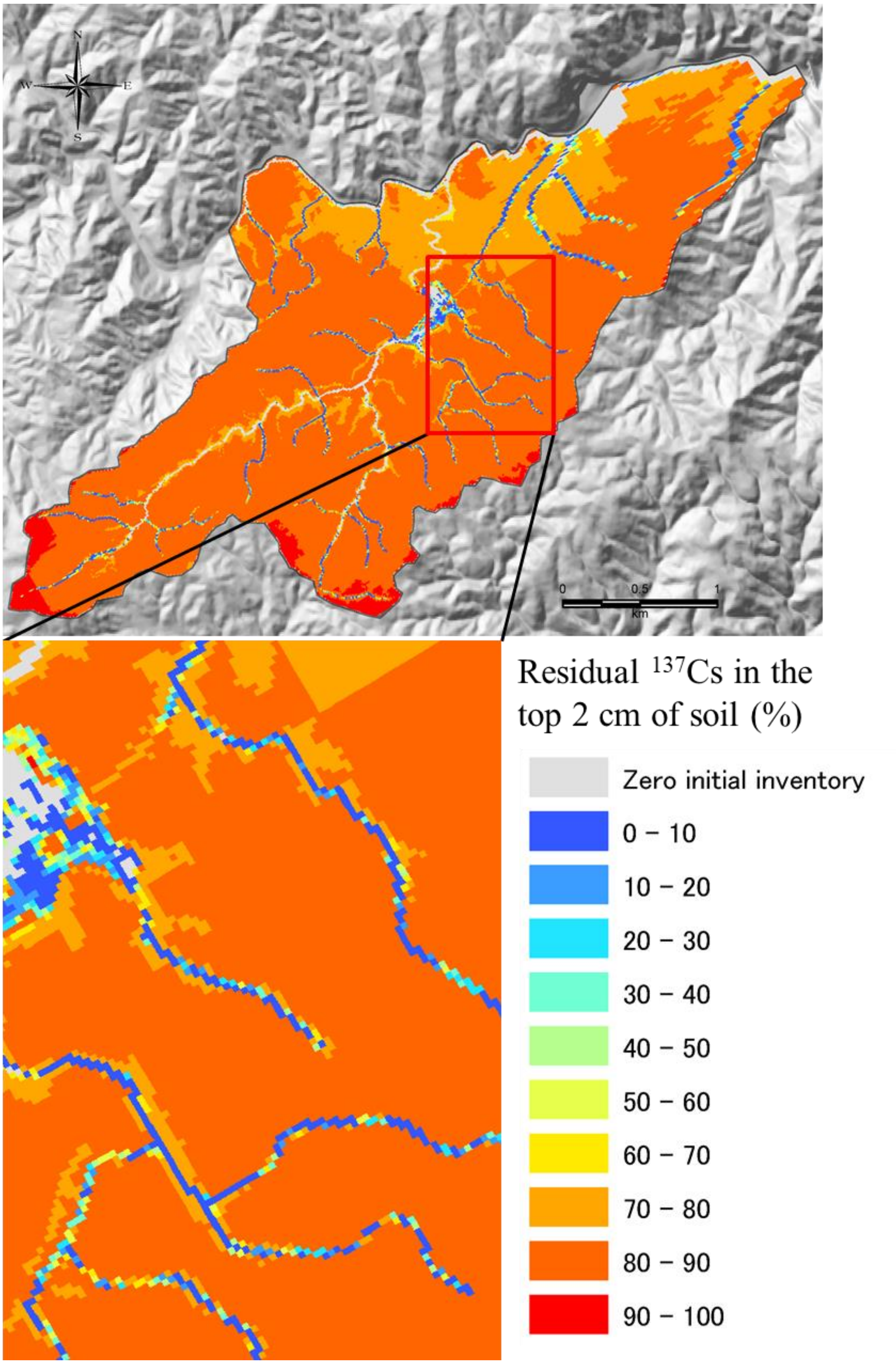
N
W
E
S
0
0.5
1
km
Residual ^{137}Cs in the top 2 cm of soil (%)
Zero initial inventory
0 – 10
10 – 20
20 – 30
30 – 40
40 – 50
50 – 60
60 – 70
70 – 80
80 – 90
90 – 100

Fig. 8

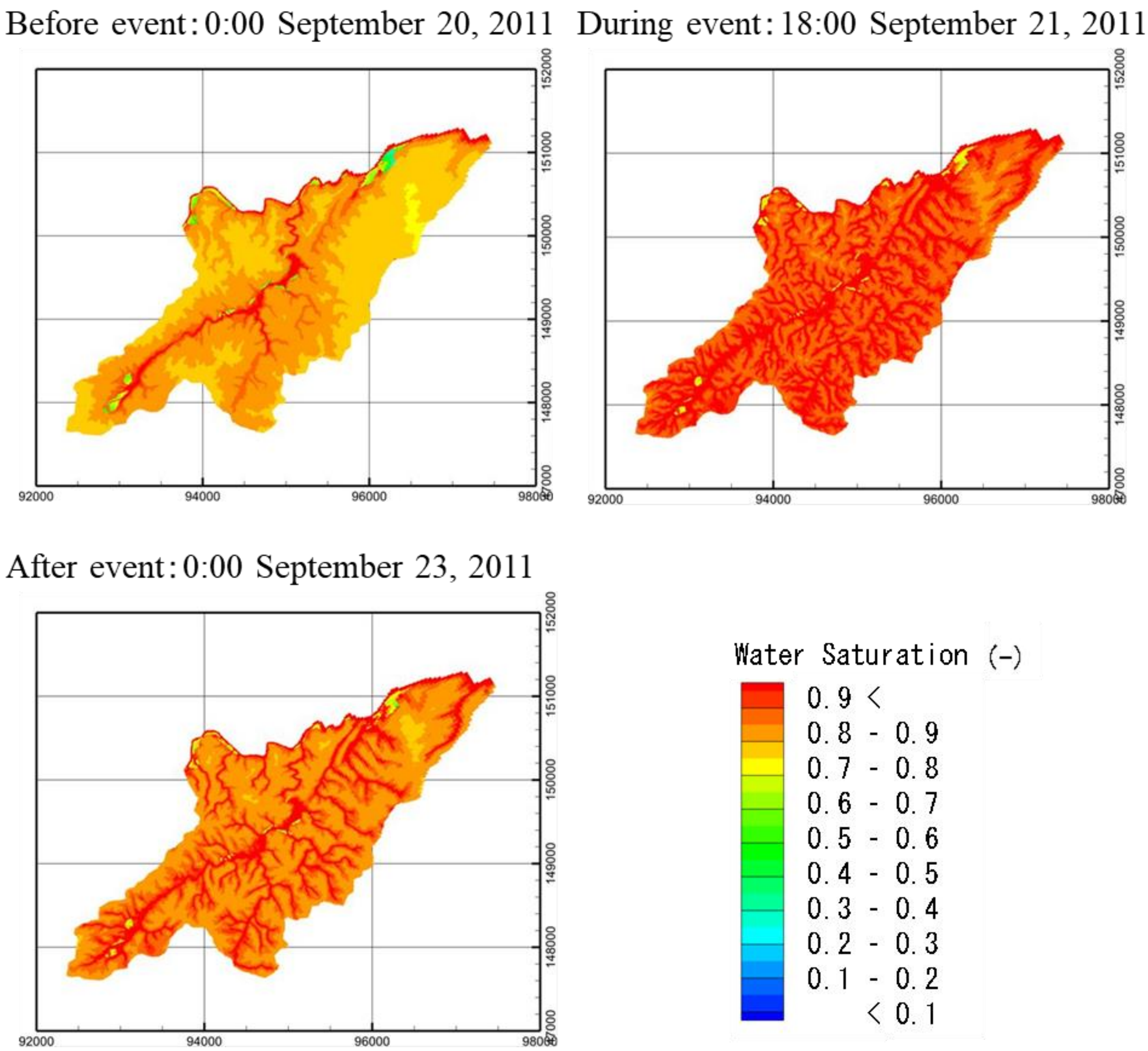
Before event: 0:00 September 20, 2011
During event: 18:00 September 21, 2011
After event: 0:00 September 23, 2011
92000
94000
96000
98000
147000
148000
149000
150000
151000
152000
Water Saturation (-)
0.9 <
0.8 - 0.9
0.7 - 0.8
0.6 - 0.7
0.5 - 0.6
0.4 - 0.5
0.3 - 0.4
0.2 - 0.3
0.1 - 0.2
< 0.1

Fig. 9

Supplementary Information

Supplementary Figures

(a)

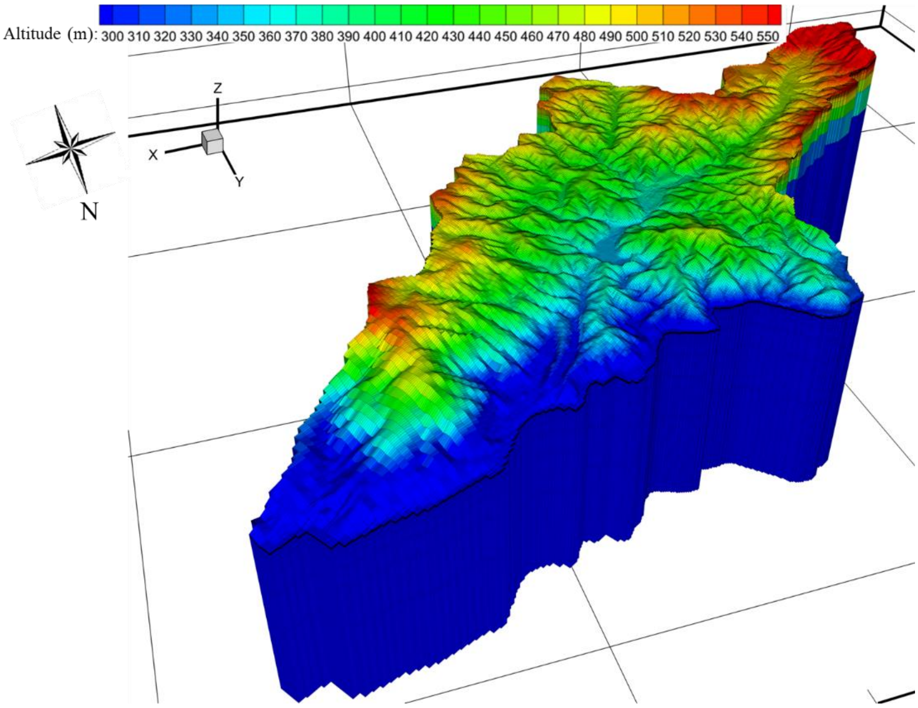

(b)

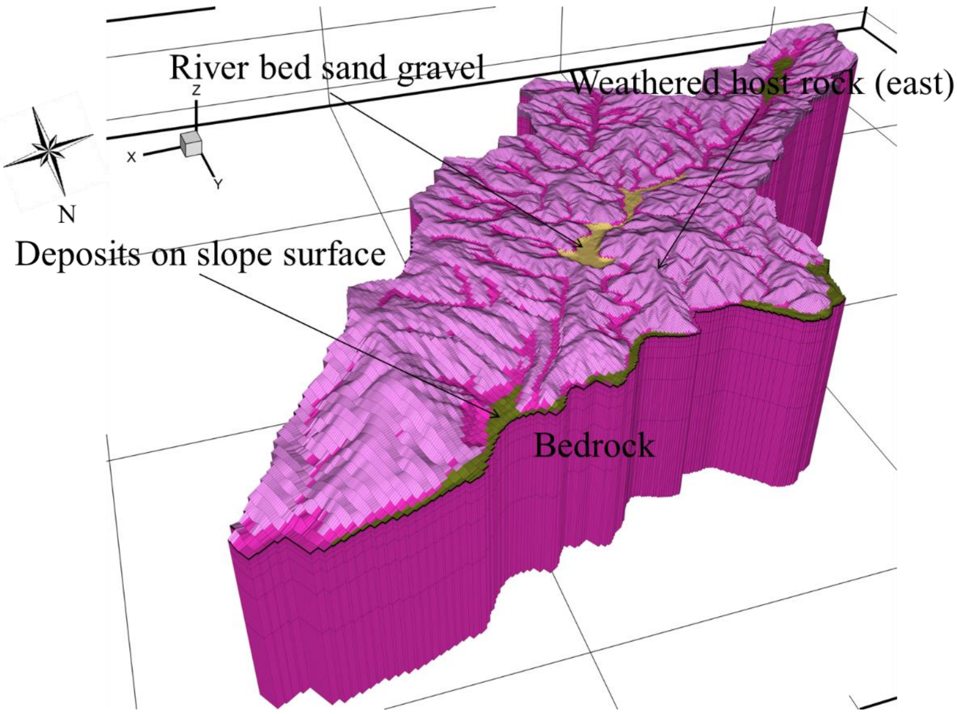

Fig. S1 Renderings of the three dimensional gird block system for the study area. Colors show (a) land surface elevation and (b) geology/deposit type.

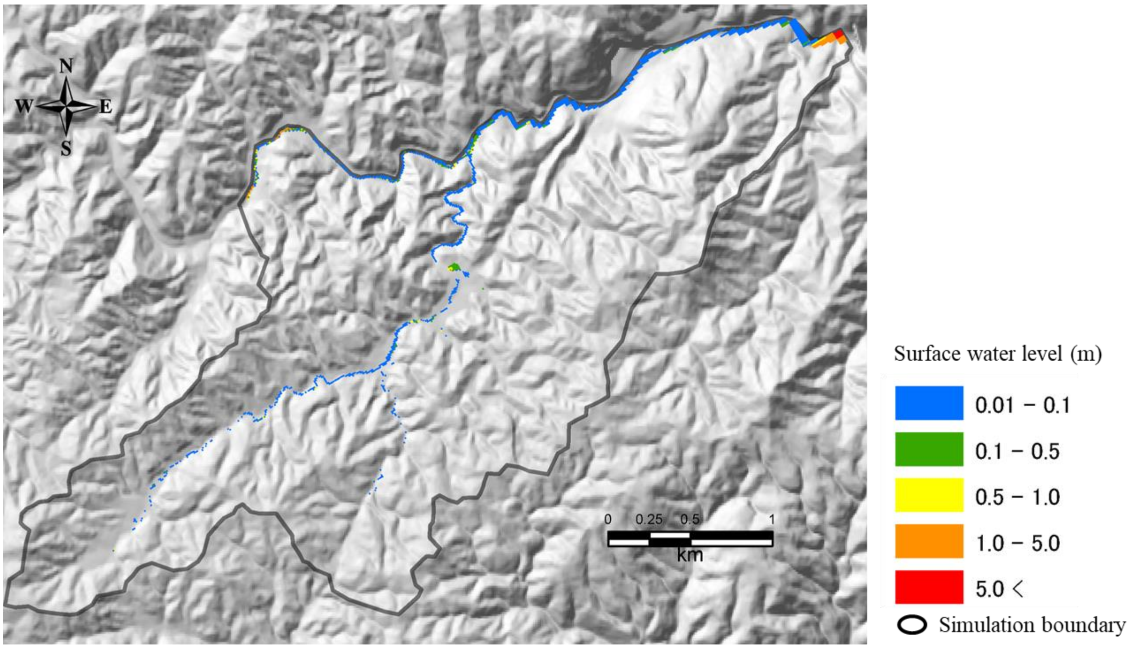

Fig. S2 Surface water level under ambient weather conditions after the equilibration simulation.

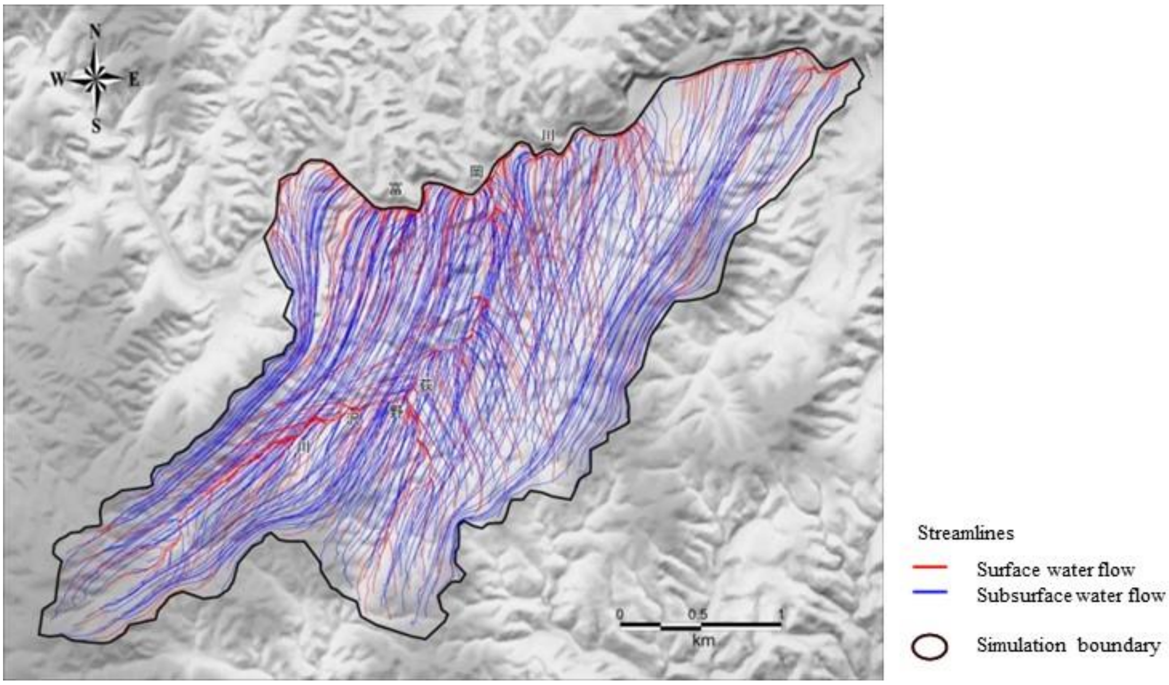

Fig. S3 Streamlines of surface and subsurface water flows under ambient conditions after equilibration.

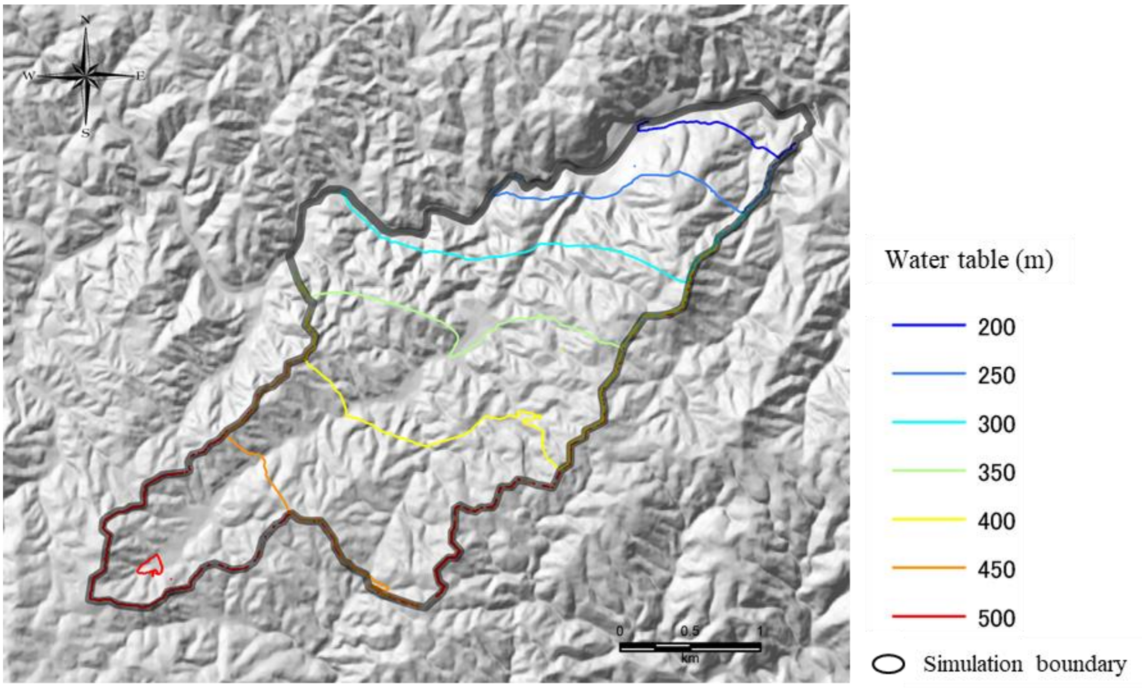

Fig. S4 Subsurface water table contours under ambient conditions.

(a)

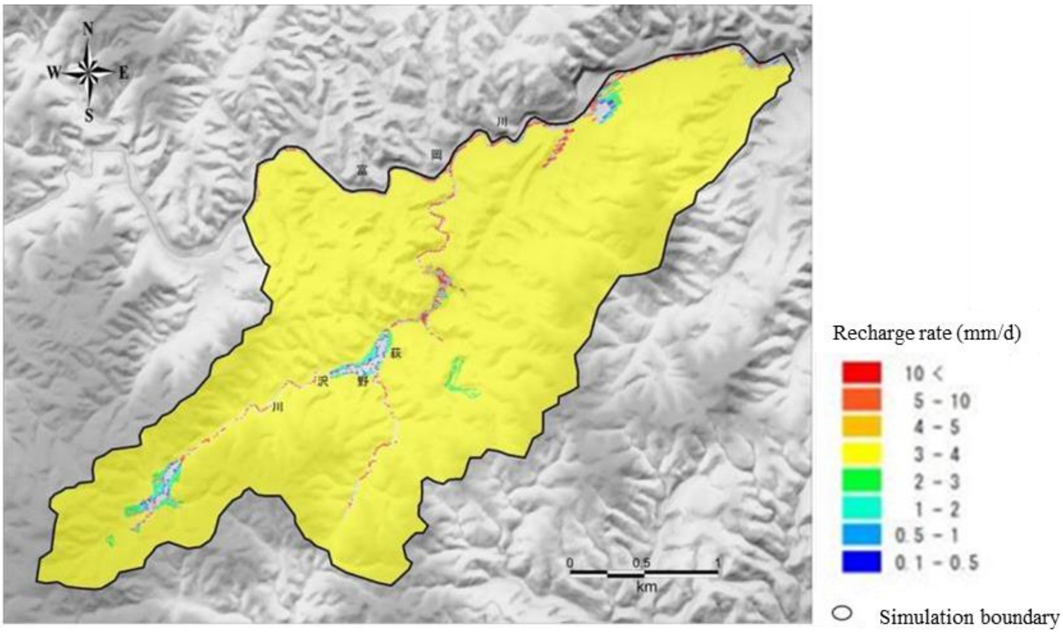

(b)

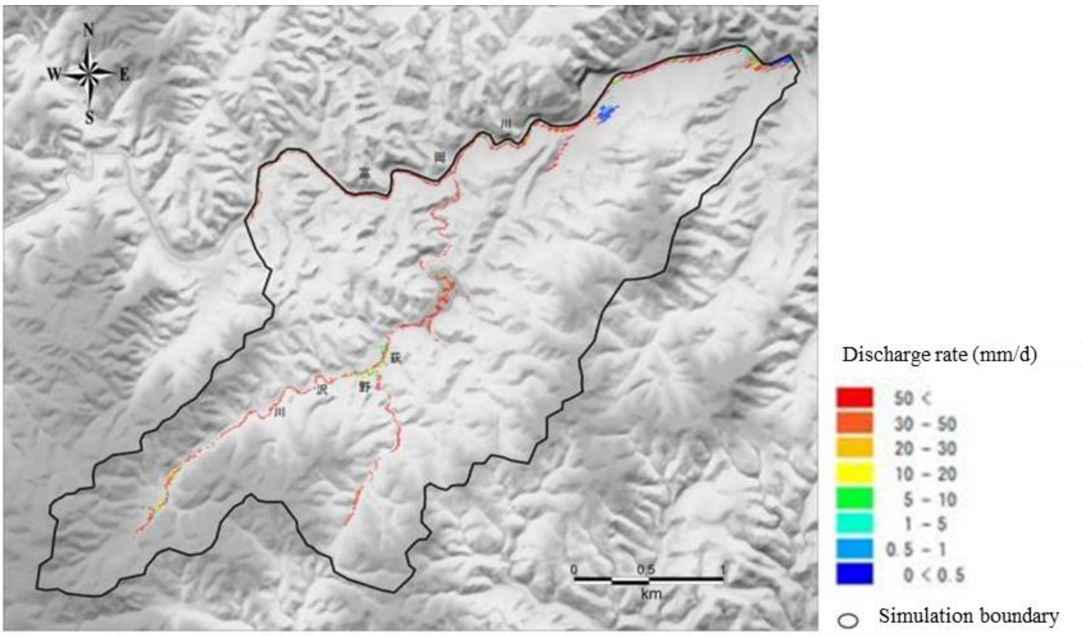

Fig. S5 (a) Recharge flux and (b) discharge flux of groundwater through the land surface in the study area under ambient conditions.

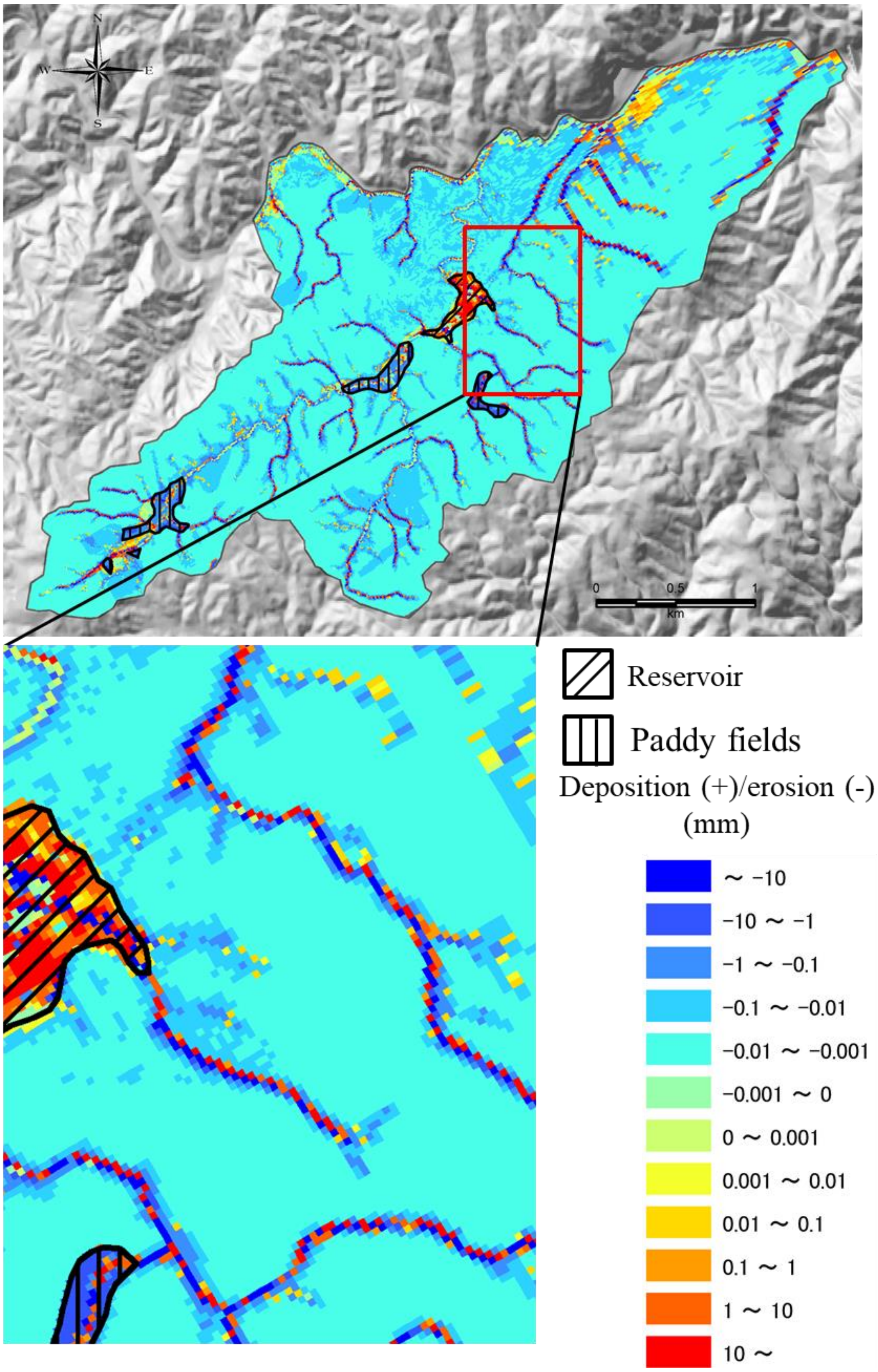

Fig. S6 Spatial distribution of the net change of soil (net deposition or erosion) between May 2011 and December 2015.

2. Supplementary Tables

Table S1: Manning's roughness coefficient for each land use and vegetation type.

Land use or vegetation type	Manning's roughness coefficient ($m^{-1/3}$ s)
Industrial sites	0.1
Paddy fields	0.2
Farmland	0.4
Felled area of forest	0.5
Coniferous forest	0.5
Deciduous broad-leaved forest	0.8
River	0.03
Reservoir	0.01

Table S2: Raindrop-induced erosion parameters.

Land use or vegetation type	Canopy height (m)	Stem storage (mm)	Crown covering (-)	Floor storage (mm)	Floor covering (-)
Industrial sites	0	0.5	0	0	0
Paddy fields	0	0.5	0.9	0	0
Farmland	0.3	0.5	0.9	0	0
Felled area of forest	0.5	0.5	0.9	0	0
Coniferous forest	15	1.5	0.8	0.25	0.95
Deciduous broad-leaved forest	15	1	0.8	0.25	0.95
River	0	0	0	0	0
Reservoir	0	0	0	0	0

Table S3: Hydraulic parameters for grid-blocks in the surface soil layers.

Land use and land cover	Subsurface	Intrinsic permeability (cm/s)	Effective porosity (-)	Relative permeability curve and capillary curve
Industrial sites		5×10^{-5}	0.25	Sandy soil
Paddy fields		1×10^{-5}	0.2	Cohesive soil
Mountains and forests, waste land, farmland	Deposit on slope surface	1×10^{-1}	0.5	Gravel soil
	Alluvium with gravel			
	Weathered host rock			Cohesive soil
Gley soil, gley lowland soil		1×10^{-5}	0.2	Cohesive soil
Andosol		1×10^{-1}	0.5	Cohesive soil

Table S4: Hydraulic parameters for grid-blocks in the subsurface layers.

Geology	Intrinsic permeability (cm/s)	Effective porosity (-)
River bed sand gravel	1×10^{-2}	0.3
Deposits on sloped surfaces	3×10^{-3}	0.3
Weathered host rock (east)	1×10^{-4}	0.2
Bedrock	1×10^{-6}	0.1

Table S5: Sediment particle size distribution.

Land use land cover	Subsurface	Sediment particle size					
		Clay	Silt	Fine sand	Sand	Large sand	Gravel
		$\Phi < 5$ μm	Φ 5 ~ 74 μm	Φ 74 μm ~ 0.25 mm	Φ 0.25 ~ 0.5 mm	Φ 0.5 ~ 2 mm	$\Phi > 2$ mm
Industrial sites		-	-	-	-	-	-
Paddy fields		0.2	0.6	0.1	0.05	0.05	-
Mountains and forests, waste land, farmland	Deposits on sloped surfaces	0.05	0.3	0.1	0.1	0.15	0.3
	Alluvium with gravel	0.05	0.15	0.1	0.1	0.2	0.4
	Weathered host rock	0.05	0.4	0.15	0.2	0.1	0.1
Gley soil, gley lowland soil		0.2	0.5	0.2	0.05	0.05	-
Andosol		0.1	0.4	0.2	0.2	0.1	-

Table S6: Soil detachment properties.

<table>
<tr><th>Land use or land cover</th><th>Subsurface</th><th>Soil Detachability Index (g/J)</th><th>Adhesion (kPa)</th></tr>
<tr><td>Industrial sites</td><td></td><td>n/a</td><td>0</td></tr>
<tr><td>Paddy fields</td><td></td><td>2.4</td><td>10</td></tr>
<tr><td rowspan="3">Mountains and forests, waste land, farmland</td><td>Deposit on sloped surfaces</td><td rowspan="2">3</td><td rowspan="2">3</td></tr>
<tr><td>Alluvium with gravel</td></tr>
<tr><td>Weathered host rock</td><td rowspan="2">2.4</td><td rowspan="2">10</td></tr>
<tr><td>Sanddune plant</td><td>Alluvium with sand</td></tr>
<tr><td>Gley soil, gley lowland soil</td><td></td><td rowspan="2">6</td><td rowspan="2">2</td></tr>
<tr><td>Andosol</td><td></td></tr>
</table>

Table S7: Thickness of 28 sub-surface layers

<table>
<tr><th>Layer</th><th>Layer thickness (m)</th><th>Type</th></tr>
<tr><td>1</td><td>0.02</td><td rowspan="6">Surface soil</td></tr>
<tr><td>2</td><td>0.1</td></tr>
<tr><td>3</td><td>0.18</td></tr>
<tr><td>4</td><td>0.23</td></tr>
<tr><td>5</td><td>0.23</td></tr>
<tr><td>6</td><td>0.23</td></tr>
<tr><td>7-28</td><td>Layers with increasing thickness with depth. Individually thicknesses depend on location</td><td>Bedrock, Weathered host rock etc.</td></tr>
</table>

Table S8

Cesium-137 activity of the settling particles collected by the sediment trap in the Ogi Dam reservoir. Errors are one standard deviation estimated from HPGe counting statistics.

Sampling period	^{137}Cs (kBq/kg)
Sept. 21-Oct. 17, 2013	9.0 ± 0.065
Dec. 18, 2013-Mar. 13, 2014	8.1 ± 0.072
Mar. 14-May 20, 2014	2.2 ±0.032
May 21-July 8, 2014	5.9 ±0.060
July 9-Aug. 7, 2014	8.8 ±0.12
Aug. 8-Sept. 11, 2014	12 ±0.12
Sept. 12-Oct. 18, 2014	16 ±0.13
Oct. 19-Oct. 30, 2014	16 ±0.21
Oct. 31, 2014-Jan. 14, 2015	14 ±0.080
Jan. 15-May 25, 2015	9.4 ±0.073
May 26-July 27, 2015	28 ±0.16
July 28-Oct. 5, 2015	13 ±0.082
Oct. 6-Nov. 30, 2015	17 ±0.091